arXiv:1703.02589v1 [cs.CV] 7 Mar 2017

Texture Classification of MR Images of the Brain in ALS using CoHOG

G M Mashrur E Elahi[a,*], Sanjay Kalra[b], Yee-Hong Yang[a]

[a] *Departments of Computing Science, University of Alberta, Canada*
[b] *Departments of Medicine, Biomedical Engineering and Computing Science, University of Alberta, Canada*

Abstract

Texture analysis is a well-known research topic in computer vision and image processing and has many applications. Gradient-based texture methods have become popular in classification problems. For the first time we extend a well-known gradient-based method, Co-occurrence Histograms of Oriented Gradients (CoHOG) to extract texture features from 2D Magnetic Resonance Images (MRI). Unlike the original CoHOG method, we use the whole image instead of sub-regions for feature calculation. Also we use a larger neighborhood size. Gradient orientations of the image pixels are calculated using Sobel, Gaussian Derivative (GD) and Local Frequency Descriptor Gradient (LFDG) operators. The extracted feature vector size is very large and classification using a large number of similar features does not provide the best results. In our proposed method, for the first time to our best knowledge, only a minimum number of significant features are selected using area under the receiver operator characteristic (ROC) curve (AUC) thresholds with $p \leq 0.01$. In this paper we apply the proposed method to classify Amyotrophic Lateral Sclerosis (ALS) patients from the controls. It is observed that selected texture features from downsampled images are significantly different between patients and controls. These features are used in a linear support vector machine (SVM) classifier to determine the classification accuracy. Optimal sensitivity and specificity are also

*Corresponding author
Email address: eelahi@ualberta.ca (G M Mashrur E Elahi)

calculated. Three different cohort datasets are used in the experiments. The performance of the proposed method using three gradient operators and two different neighborhood sizes is analyzed. Region based analysis is performed to demonstrate that significant changes between patients and controls are limited to the motor cortex. The proposed method is compared with that of the gray level co-occurrence matrix (GLCM) method. The experimental results show that our proposed method outperforms that of the GLCM.
Keywords: Texture Analysis; Oriented Gradients and co-occurrence matrix; co-occurrence histograms of oriented gradients; MRI images of Amyotrophic Lateral Sclerosis (ALS).

---

1. Introduction

Texture analysis is a well-known and promising topic in image processing and computer vision, has been a major research topic for the last four decades, and more recently has been considered for medical imaging applications Kassner and Thornhill (2010). Its applications include document processing Zhao et al. (2010) , remote sensing Santos et al. (2012), automated inspection Li and Tsai (2012), fingerprint identification Nanni and Lumini (2008), and medical image analysis Lehana et al. (2012).

In texture analysis, texture features that are invariant to geometric transformation, noise, blurriness, and illumination changes are desired. Some well-known 2D texture methods are the Run Length Matrix (RLM) Galloway (1975), filter responses in the frequency Chu and Chan (2009) and spatial Leung and Malik (2001), Varma and Zisserman (2005) domains, Wavelets Unser and Eden (1989), Orientation Pyramid Reyes-Aldasoro and Bhalerao (2006), Markov Random Fields (MRFs) Cross and Jain (1983), Gaussian MRFs Cohen et al. (1991), spin images Lazebnik et al. (2005), the Local Binary Patterns (LBP) Ojala et al. (2002) and its variants, gray level co-occurrence matrix (GLCM) Haralick et al. (1973), and the gray level Aura matrix (GLAM) Qin and Yang (2004). However, none of the above methods are insensitive to illumination changes.

Recently, gradient orientation based texture methods have become popular in computer vision and image processing. Among them Scale Invariant Feature Transform (SIFT) Lowe (2004), Histograms of Oriented Gradients (HOG) Dalal and Triggs (2005) and Co-occurrence Histograms of Oriented gradients (CoHOG) Watanabe et al. (2009) are commonly used in object detection. The CoHOG method and its variants Kataoka et al. (2014), Hanbay et al. (2015) have been successfully used in pedestrian detection Watanabe et al. (2009), face recognition Do and Kijak (2012) , fine-grained activity recognition Kataoka et al. (2014), etc.

In recent years, texture analysis methods have been used in medical imaging studies that include texture analysis of MRI images. In particular, in the diagnosis of dementia using GLCM and Gabor filter responses Sivapriya et al. (2011), the study of pathological changes of the hippocampus in patients with Alzheimer's disease and mild cognitive impairment using GLCM and RLM Li et al. (2010), brain tumor detection Kharrat et al. (2009) and the study of epilepsy using wavelet features Jafari-Khouzani et al. (2003) are some important contributions. Also a 3D texture analysis in biomedical imaging is proposed in Depeursinge et al. (2014). Texture analysis is used in optical projection tomography images to discriminate colorectal polyps Li et al. (2015) and a scale invariant texture recognition methods are applied for the computer assisted diagnosis of celiac disease in Hegenbart et al. (2013).

Amyotrophic Lateral Sclerosis (ALS) is a fatal progressive neurodegenerative disorder of adulthood that causes rapid muscular weakness and disability. It affects both the upper motor neurons (UMN) of the cerebral cortex and the lower motor neurons (LMN) in the brainstem and spinal cord Kiernan et al. (2011). Currently, there is no reliable tool to provide a quantitative measure of cerebral degeneration in ALS and such a tool is desperately needed to aid in diagnosis and to evaluate novel therapies. A 2D region of interest based approach was used to find texture changes in ALS Albuquerque et al. (2016). GLCM has been used for 3D texture analysis in ALS Maani et al. (2016). However, the sensitivity and specificity of these methods are suboptimal. Therefore, improved

sensitivity and specificity and classification accuracy are required.

In this paper, we adopt the well-known CoHOG method for the first time to extract features in the detection of ALS. In the original CoHOG method, a given image is first subdivided into regions from which features are extracted. In this paper, CoHOG is applied to the whole image for feature extraction at different resolutions. Some well-known methods such as Sobel Duda et al. (1973), Gaussian Derivative (GD) filters Hanbay et al. (2015) and Local Frequency Descriptor Gradient (LFDG) operators Maani et al. (2014), Maani et al. (2013) are used to calculate the gradient orientations of the image pixels. The gradient orientations of the pixels are then quantized into N bins. The co-occurrences of the gradients are summed for each offset and stored into an $N \times N$ co-occurrence matrix. An offset is defined by a distance and a direction. Offsets are limited to within a radius specified from the pixel. All the co-occurrence matrices calculated from all the offsets are combined to create the feature vector (FV). The size of the FV can be very large depending on the number of offsets. Because not all features are significant, we apply receiver operator characteristic (ROC) curve analysis to select significant features. The size of the resulting feature vector (SFV) is smaller than the original FV size. We employ a linear support vector machine (SVM) Cortes and Vapnik (1995) classifier to calculate the classification rate between patients and controls. An ROC analysis of comparing different downsampled resolutions of the same image is done and also the performance of the proposed method using two different neighborhood sizes and three different gradient operators is analyzed. As well, we subdivide the image to perform a region based analysis to identity the regions with significant changes between the patients and the controls.

The main contributions of this paper include the use of the whole image for feature extraction to reduce the sub-region issue problem. Two well-known gradient operators are used for the first time for gradient calculation with a larger neighborhood to evaluate the effect of using more global information for co-occurrence calculation on classification accuracy. To the best of our knowledge, we are the first to use a feature selection method to extract CoHOG features

using an AUC threshold. Experimental results show that classification using feature selection has a better accuracy with a higher neighborhood size.

The rest of the paper is organized as follows. Related works are discussed in Section 2. In Section 3, we explain the proposed approach of feature extraction. The experimental results and discussions are presented in Section 4. Section 5 concludes the paper.

2. Related Works

Texture analysis is a promising topic in computer vision and image processing. Visual patterns appearing in images are called image textures and can be seen everywhere such as: carpet, wall, ultrasound images, fingerprint images, and medical images. Texture analysis characterizes and quantifies pattern variations in images, including those that are imperceptible to the human eye.

Two dimensional texture analysis methods have been used for document processing Zhao et al. (2010), remote sensing Santos et al. (2012), automated inspection Li and Tsai (2012), fingerprint identification Nanni and Lumini (2008), medical image analysis Lehana et al. (2012), etc. Some of the important 2D methods are discussed below.

The Run Length Matrix (RLM) Galloway (1975) is used to calculate features of different terrain types. Gabor filtering banks are used in filtering responses in the frequency Chu and Chan (2009) and spatial Leung and Malik (2001), Varma and Zisserman (2005) domains for image texture recognition. Multiresolution Wavelets Unser and Eden (1989) are used in texture feature extraction and selection to segment textures. A Markov Random Fields (MRFs) Cross and Jain (1983) model is used to analyze textures in images. Some related methods include the Gaussian MRFs Cohen et al. (1991) and spin images Lazebnik et al. (2005). Another multiresolution approach to gray-scale and rotation invariant texture classification based on Local Binary Patterns (LBP) and its variants are presented in Ojala et al. (2002).

In Gray Level Co-occurrence Matrix (GLCM) Haralick et al. (1973), image

intensities are quantized into a fixed number of gray levels and a co-occurrence matrix is formed by summing the co-occurrences of a specific pair of gray levels. Recently, GLCM has been used in medical imaging such as diagnosis of dementia Sivapriya et al. (2011), the study of pathological changes of hippocampus in patients with Alzheimer's disease and mild cognitive impairment Li et al. (2010), and brain tumor detection Kharrat et al. (2009). The limitation of GLCM is that it works with the intensity levels of gray scale images, which will have unpredictable performance when the acquisition equipment changes.

Gradient orientation based texture methods have become popular in recent years for their robustness against image intensity changes, blurriness and deformations. Histograms of Oriented Gradients (HOG) Dalal and Triggs (2005) and Co-occurrence Histograms of Oriented gradients (CoHOG) are two such commonly used methods that have been used for objects detection Dalal and Triggs (2005), pedestrian detection Watanabe et al. (2009), face recognition Do and Kijak (2012), fine-grained activity recognition Kataoka et al. (2014), etc. We give a brief description of HOG and CoHOG below.

2.1. Histograms of Oriented Gradients (HOG)

The HOG method uses a gradient oriented image as input. The gradient orientations are quantized into N bins. Then the image is subdivided into M number of equal sub-regions. For each sub-region, a histogram of orientations is computed. The size of the histogram is N. For M sub-regions, there are M different histograms each of size N. Finally, these histograms are concatenated to form the feature vector histogram of size $M \times N$. The limitation of HOG is that it only counts the orientations in a local region. Inter-relationship information between orientations is not captured. To overcome this limitation, an improvement of HOG called the Co-occurrence HOG (CoHOG) method is proposed.

2.2. Co-occurrence HOG (CoHOG)

CoHOG is an extension of HOG. It also uses the quantized gradients as input and subdivides the image into a number of sub-regions. CoHOG uses a

circular neighborhood with a given radius in which each pixel with the center pixel forms a pair called an offset. Now for each sub-region and for each offset, the co-occurrences of an orientation pair is computed by scanning all the pixels in the sub-region to form a co-occurrence matrix (CM). The size of the CM is $N \times N$, where N is the number of distinct orientations. The total number of CMs for a sub-region depends on the number of offsets. Finally, these CMs are concatenated to form the histogram for the sub-region. Then, the histograms of all the sub-regions are concatenated to form the CoHOG feature vector for the given image. The feature vector size depends on the number of orientations, the number of offsets and the number of sub-regions. For example, if an image has M sub-regions and K offsets with a CM size of $N \times N$, then the final feature vector size is $M \times K \times (N \times N)$.

The CoHOG method has the advantages over HOG in capturing the inter-relationship among the neighboring pixel orientations and, by using different offsets, the co-occurrence matrices can better represent the local and global orientation information. The use of sub-regions limits the accuracy of CM for boundary pixels and thus some information is incomplete for each sub-region.

In this paper, we present a modified CoHOG method for texture feature extraction of the whole image which can overcome the sub-region issue mentioned above and can reduce the feature vector size.

3. Proposed Method

The original CoHOG method uses sub-regions of an image and calculates the sum of the co-occurrences of orientation pairs. The use of a sub-region limits the accuracy of co-occurrence calculation for the boundary pixels and thus some information is incomplete for each sub-region. We have used the simple approach of applying CoHOG to the whole image using the three proposed gradient methods for texture feature extraction.

The CoHOG features are extracted using two different neighborhood sizes. The original CoHOG method uses a maximum neighborhood size of 4. We use

a larger neighborhood size of 8 to evaluate the effect of using more distance information for co-occurrence calculation on classification accuracy.

The extracted CoHOG feature vector size is very large. Image classes that contain very small changes in between the groups are almost similar in all other regions. Features extracted from these regions are also similar. Using this large number of similar features creates ambiguity in defining the optimal hyperplane and leads to an incorrect classification by a classifier. Thus, we select significant features using area under the ROC curve (AUC) analysis for classification, and only features that contain significant differences in between the classes are selected using an AUC threshold.

The proposed method consists of four steps (see Fig. 1): pre-processing, texture feature extraction, feature selection and classification. These steps are discussed below.

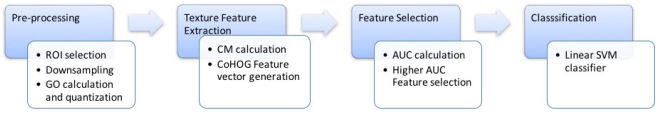

Figure 1: Overview of our proposed approach.

3.1. Pre-processing

Texture features are extracted from pre-processed MRI images. Pre-processing involves region of interest (ROI) selection, downsampling, gradient orientation (GO) calculation and quantization.

3.1.1. ROI Selection

From the MRI scan of the whole brain, coronal slices with an angulation parallel to the corticospinal tract (see Fig. 2 (a)) are used for texture feature calculation (see Fig. 2 (c)).

In particular, an ROI is manually defined that includes the region above the inferior horn of the lateral ventricles (see Fig. 3).

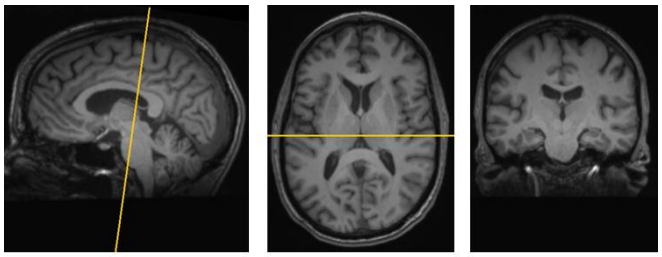

Figure 2: (a) Sagittal, (b) Axial and (c) Coronal image slices. Coronal imaging is used in texture feature extraction.

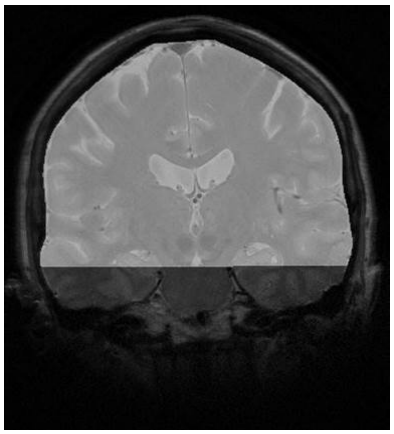

Figure 3: ROI selection from a coronal image slice. The highlighted regions are selected as ROI.

3.1.2. Downsampling

The selected ROI is downsampled to four different resolutions. The scaling factors are $0.5, 0.25, 0.167$ and 0.125. These scaling factors are chosen to down sample the ROI into $1{\times}1$ mm^2, $2{\times}2$ mm^2, $3{\times}3$ mm^2 and $4{\times}4$ mm^2 physical dimensions, respectively.

3.1.3. GO Calculation and Quantization

The gradient orientations of image pixels are computed by convolving the gradient operators with the image. Horizontal and vertical gradient operators are used to calculate the corresponding gradient images and then gradient orien-

tations are calculated from the gradient images. The gradient orientation (GO) of an image pixel is calculated using three different methods, namely, Sobel Duda et al. (1973), Gaussian Derivative (GD) Hanbay et al. (2015) and Local Frequency Descriptor Gradient (LFDG) Maani et al. (2014).

Sobel uses two 3×3 kernels to estimate the horizontal and vertical derivatives. The two operators used in this method are shown in Eq. 1,

$$G_x = \begin{bmatrix} -1 & 0 & 1 \\ -2 & 0 & 2 \\ -1 & 0 & 1 \end{bmatrix}, G_y = \begin{bmatrix} -1 & -2 & -1 \\ 0 & 0 & 0 \\ 1 & 2 & 1 \end{bmatrix}, \tag{1}$$

where G_x and G_y are the corresponding horizontal and vertical gradient operators.

The GD operators that use two basic one-dimensional derivative filters are given in Eq. 2 Hanbay et al. (2015), Zhang et al. (2013),

$$f_1(t) = \frac{-2t}{\sigma^2} e^{-\frac{t^2}{\sigma^2}}, f_2(t) = e^{-\frac{t^2}{\sigma^2}}, \tag{2}$$

where t is the width of the derivative filter and σ the standard deviation. These one-dimensional derivatives are used to calculate the two horizontal and vertical derivative filters as shown below Hanbay et al. (2015), Zhang et al. (2013).

Basic filters	Filter in x	Filter in y
G_x	f_1	f_2
G_y	f_2	f_1

Here, f_1 and f_2 are two vectors defined in Eq. 2. For both the G_x and G_y filters, filter in x and filter in y, are convolved with each column and each row of an image I, respectively, to form the corresponding gradient image.

The LFDG operators can be calculated using the representation as shown in Eq. 3 and Eq. 4 Maani et al. (2014),

$$G_x = \sum_{k=1}^{p} f_k cos\left(\frac{2\pi(k-1)}{p}\right), \tag{3}$$

$$G_y = \sum_{k=1}^{p} f_k cos\left(\frac{\pi}{2} + \frac{2\pi(k-1)}{p}\right), \tag{4}$$

where p is the number of neighboring points and f_k the corresponding gray level of the kth neighbor.

The kernel size depends on the specified radius. For a kernel with radius R, the LFDG operator has the kernel size of $N \times N$, where $N = 2R + 1$. In our experiments, we use $R = 1$ and 34 neighboring points to calculate the kernel operators.

For all of the operators discussed above, G_x and G_y are convolved with the original image to compute the horizontal and vertical gradient images, respectively. Gradient orientations are computed using Eq. 5,

$$GO = arctan\frac{G_y}{G_x}. \tag{5}$$

Finally, the orientations are quantized into 8 bins. In particular, $0^\circ - 360^\circ$ orientations are divided into eight bins of 45° each. Each pixel's orientation is assigned to the nearest bin.

3.2. Feature Extraction

The quantized oriented image is used for feature extraction using the CoHOG method. It is a two step process. First, all the co-occurrence matrices for all the offsets are computed and then these matrices are combined to obtain the feature vector.

3.2.1. Co-occurrence Matrix (CM) Calculation

In CoHOG, an offset corresponds to the center pixel of the neighborhood to one of its neighbors (see Fig. 4 (b)). Fig. 4 (a) shows a neighborhood with a radius of size 4, 6, and 8 from the center green pixel. For a given radius, each neighbor within the radius is paired with the green pixel to form an offset. For example, using a neighborhood size of 4 we have a total of 31 offsets including the pair of the green pixel with itself. Increasing the neighborhood size increases the number of offsets and thus the number of CMs. The upper half of the circular

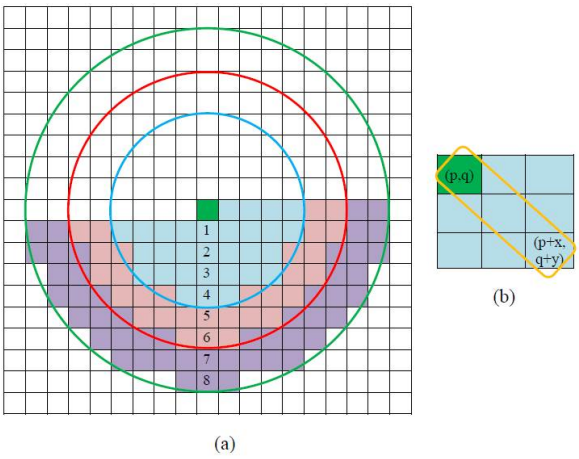

Figure 4: (a) Offsets for different radii and (b) a specific offset at distance (x, y) from pixel (p, q).

neighborhood is not considered because they are redundant since pixels in the top left corner of the image are processed first.

In our proposed approach, we use the whole image for co-occurrence matrix calculation instead of using sub-regions as that used in the original CoHOG method. A neighborhood size of 4 and 8 are separately used for feature extraction. In CoHOG, the co-occurrence matrix is obtained by summing the co-occurrences of each pair of orientations for each offset. The size of the co-occurrence matrix is $N \times N$, where N is the number of distinct orientations which is pre-defined. For a specific offset (x, y) and a specific orientation at pixel $(p, q) = i$ and pixel $(p + x) = j$, the equation for calculating the CM is shown in Eq. 6 Watanabe et al. (2009),

$$CM_{x,y}(i,j) = \sum_{p=1}^{m}\sum_{q=1}^{n}\begin{cases} 1 \text{ if } Q \text{ is True} \\ 0 \text{ Otherwise} \end{cases}, \tag{6}$$

where $Q = GO(p, q) = i$ and $GO(p + x, q + y) = j$ and $GM(p, q) \geq T$ and $GM(p + x, q + y) \geq T$. Here $m \times n$ is the size of the gradient oriented image I. GM is the gradient magnitude of the corresponding pixel and T is the threshold magnitude to consider for the co-occurrence count.

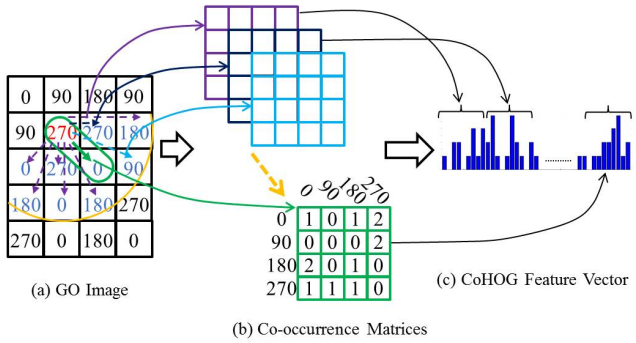

Figure 5: Illustration of the Co-occurrence Histograms of Oriented Gradients (CoHOG) method.

Fig. 5 shows the workflow of CoHOG. It shows that using the gradient oriented image of four different orientations, a co-occurrence matrix of size 4×4 for each offset within the specified radius is created. The method scans each pixel for all the offsets and sums the co-occurrences of the orientations for that offset and stores the sums into the entry that corresponds to the pair of orientations of the co-occurrence matrix. After scanning all the pixels, it finishes in building up all the co-occurrence matrices.

3.2.2. Feature Vector Generation

Now all the created CMs are used to generate the feature vector for the selected image. The feature vector (FV) is generated by concatenating the CMs as shown in Eq. 7,

$$FV = \Big\|_{i=1}^{K} vec(CM_i) \tag{7}$$

where, $\|$ is the concatenation operator, K is the number of offsets and vec is the vector representation of CM. The FV is a histogram of the co-occurrences of orientations of different offsets in the image (see Fig. 5(c)).

The size of the feature vector depends on the number of offsets used and the

size of the CM as shown in Eq. 8,

$$FV \text{ size} = \text{number of offsets} \times \text{size of CM}. \tag{8}$$

One can see that the size of the feature vector is very large if the number of offsets is large. For example, with a neighborhood size of 4, the total number of offsets is 31. Then the CM size is $8\times8 = 64$, and the FV size = $31\times64 = 1984$. With the same CM size, if the radius is increased to 6 with 61 offsets and 8 with 109 offsets then FV size = 3904 and FV size = 6976, respectively. When the FV size is large, it is difficult to distinguish between two classes of distinct categories. Changes occur in a small portion of the images between two classes and thus the features of all other portions of the image classes are almost similar. Distinguishing between classes is difficult due these similar features. Therefore, it is important to select those significant features that are extracted from the changed portion of the images. These selected features have significant differences between the classes and are used for classification.

3.3. Feature Selection

ROC based methods Serrano et al. (2010), Ma and Huang (2005), Lorente et al. (2013), are well-known and promising in selecting important features. Some of the ROC based feature selection examples include feature ranking and significant feature selection using area under the ROC curve analysis Serrano et al. (2010), a regularized ROC method for disease classification and biomarker selection for microarray data Ma and Huang (2005), comparison of the ROC feature selection method with other popular methods Lorente et al. (2013) and feature selection using the ROC curve for small samples and imbalanced data classification problems Alshawabkeh et al. (2011). These methods demonstrate better classification accuracy using the ROC feature selection approach.

In this paper, feature selection is performed using ROC analysis. It is noteworthy that we are the first to use a feature selection method to extract significant CoHOG texture features to further improve classification accuracy. Significant features are selected using area under the ROC curve (AUC) analysis for

classification. Only features that contain significant differences in between the classes are selected using an AUC threshold. In the experiments, better results are found with features selected using AUC ≥ 0.8 with a significance level of $p \leq 0.01$.

3.4. Classification

For classification we use a linear support vector machine (SVM) Cortes and Vapnik (1995). A two stage classification is used with the use of training and testing datasets. For a two class classification, the SVM computes the optimal hyperplane to partition the feature space of the training samples into two halves. Samples from both classes are used for training and then using the trained model, we test the classification accuracy of unknown classes.

4. Experimental Results

In this section, we discuss the results using the proposed method for three datasets. The proposed method is implemented in Matlab. The program runs on a PC with an Intel Core i7 with 3.40GHz CPU with 24GB RAM running Windows 7 Professional.

4.1. Datasets

We use three datasets of MRI imaging of ALS patients and healthy controls. These datasets are acquired using two different scanning machines with different scanning parameters for each datasets. All the subjects are different in all the datasets. Also image resolution and contrast are different for each dataset.

All patients are clinically probable or definite sporadic ALS according to the revised El Escorial criteria Brooks et al. (2000) were recruited. All patients had clinical evidence of UMN and LMN involvements. The details of the subjects are discussed below.

Table 1: Details of the subjects for Dataset 1

Subjects	No.	Average Age	Male	Female
Patients	12	58 ± 11	7	5
Controls	19	57 ±11	8	11

4.1.1. Dataset 1

Twelve patients and nineteen controls are in this datasets. Details of the patients and controls for this dataset are given in Table 1.

MR imaging was performed on a 4.7 Tesla whole-body scanner (Varian Unity Inova console). High-resolution fast spin echo T2-weighted images were acquired in the coronal plane (TR = $4000ms$, TE = $33.3ms$, pixel size = $0.5 \times 0.5mm^2$, slice thickness = $2mm$).

2D MR images of the subjects are downsampled into four different resolutions. Details of the downsampled images are given in Table 2.

Table 2: Details of the downsampled 2D MR images of the subjects for Dataset 1 and Dataset 3

Scale Factor	Pixel size (mm^2)	Image size ($Pixel^2$)
1	0.5 × 0.5	385 × 512
0.5	1 × 1	192 × 256
0.25	2 × 2	96 × 128
0.167	3 × 3	64 × 85
0.125	4 × 4	48 × 64

4.1.2. Dataset 2

Nineteen patients and twenty controls are in this dataset. Details of the patients and controls are given in Table 3.

MRI scan were done on a 1.5 Tesla system (Magnetom Sonata, Siemens Medical Systems). Coronal T2-weighted images were acquired (TR=$7510ms$, TE=$113ms$, pixel size = $1.1 \times 0.9mm$, slice thickness = $5mm$).

Table 3: Details of the subjects for Dataset 2 and Dataset 3

Subjects	No.	Average Age	Male	Female
Patients	19	57±14	10	9
Controls	20	57±13	9	11

Dataset 2 MR images are downsampled into four resolutions. Details of the image resolutions for each scale are given in Table 4.

Table 4: Details of the downsampled 2D MR images of the subjects for Dataset 2

Scale Factor	Pixel size (mm^2)	Image size ($Pixel^2$)
1	0.86×0.86	208×256
0.86	1×1	178×220
0.43	2×2	89×110
0.285	3×3	59×72
0.215	4×4	44×55

4.1.3. Dataset 3

All the subjects are the same for dataset 2 and dataset 3 (see Table 3). But dataset 3 was acquired with a T1-weighted MPRAGE (TR=1600ms, TE=3.8ms, TI=1100ms, pixel size = $1.0 \times 1.0mm$, slice thickness = $1.5mm$). MRI scanning were performed on a 1.5 Tesla system (Magnetom Sonata, Siemens Medical Systems). The resolutions of downsampled images are given in Table 2.

For all the datasets, coronal imaging was performed with an angulation parallel to the corticospinal tract (see Fig. 2). An ROI was manually selected for each subject that covers the region above the inferior horn of the lateral ventricles. A sample ROI is shown in Fig. 3.

4.2. ROC Analysis of Datasets

For the three datasets we have done ROC analysis to find the area under the ROC curve (AUC) with a significance level of $p \leq 0.01$. Then classification of the subjects in the dataset using a linear SVM classifier is performed. Each

time, half of the patients and controls that are randomly selected in each dataset are used for training and those that are not selected are used for testing. The average classification accuracy and optimal sensitivity and specificity over 1000 runs are recorded. The details of the ROC analysis and classification results are discussed below.

4.2.1. ROC Analysis of Dataset 1

Six patients and ten controls are used to train the linear SVM classifier and the rest of the patients and controls are used for testing in this dataset. The maximum AUC is calculated for the selected features and then the classification accuracy is calculated using the selected features. The results are shown in Table 5 and 6.

Table 5: ROC analysis of Dataset 1 using CoHOG features extracted for neighborhood radius of 4.

Image Pixel Size (mm^2)	Maximum AUC	Optimal Sensitivity	Optimal Specificity	Classification Accuracy
0.5×0.5	0.815	54%	67%	63.00%
1×1	0.895	57%	73%	67.30%
2×2	0.886	81%	84%	83.50%
3×3	0.895	81%	91%	**87.30**%
4×4	0.842	71%	84%	79.00%

Four different downsampled images along with the original image are used in this experiment. From the results it is shown that features extracted (using both neighborhood size of 4 and 8) from downsampled image (scale factor = 0.167) have better classification accuracy with a higher maximum AUC than that using the original image resolution. In particular, the best classification accuracy (93%), the maximum AUC (0.917) and the optimal sensitivity (91%) and specificity (95%) are found in features extracted using neighborhood size of 8.

Table 6: ROC analysis of Dataset 1 using CoHOG features extracted for neighborhood radius of 8.

Image Pixel Size (mm^2)	Maximum AUC	Optimal Sensitivity	Optimal Specificity	Classification Accuracy
0.5×0.5	0.831	50%	61%	57.00%
1×1	0.895	57%	74%	67.70%
2×2	0.906	74%	83%	79.30%
3×3	0.917	91%	95%	**93.00**%
4×4	0.921	90%	89%	90.30%

4.2.2. ROC Analysis of Dataset 2

In this dataset, we use 19 patients and 20 controls for classification and ROC analysis. Ten patients and 10 controls are used for training the linear SVM and the other 9 patients and 10 controls are used for testing the classification accuracy. The classification results for different downsampled images with two neighborhood sizes are shown in Table 7 (four neighbors) and Table 8 (eight neighbors).

Table 7: ROC analysis of Dataset 2 using CoHOG features extracted for neighborhood radius of 4.

Image Pixel Size (mm^2)	Maximum AUC	Optimal Sensitivity	Optimal Specificity	Classification Accuracy
0.86×0.86	0.783	48%	57%	53.30%
1×1	0.791	54%	59%	56.70%
2×2	0.810	63%	78%	71.00%
3×3	0.834	75%	78%	76.90%
4×4	0.856	84%	86%	**85.30**%

We observe from the results that downsampling increases the classification accuracy along with sensitivity and specificity. Here we found the best classification accuracy (90.40%), the maximum AUC (0.867) and with the best optimal sensitivity (92%) and specificity (88%) in downsampled images (image pixel size

Table 8: ROC analysis of Dataset 2 using CoHOG features extracted for neighborhood radius of 8.

Image pixel Size (mm^2)	Maximum AUC	Optimal Sensitivity	Optimal Specificity	Classification Accuracy
0.86×0.86	0.834	55%	60%	57.70%
1×1	0.855	60%	61%	61.10%
2×2	0.850	66%	78%	72.70%
3×3	0.834	77%	82%	80.00%
4×4	0.867	92%	88%	**90.40**%

$= 4 \times 4\ mm^2$) with a neighborhood size of 8.

4.2.3. ROC Analysis of Dataset 3

Dataset 3 is a T1-weighted dataset of the same subjects as dataset 2. Similar experimental settings are used for this dataset as the other two. The observed ROC analysis and classification results are shown in Table 9 (four neighbors) and Table 10 (eight neighbors).

Table 9: ROC analysis of Dataset 3 using CoHOG features extracted for neighborhood radius of 4.

Image Pixel Size (mm^2)	Maximum AUC	Optimal Sensitivity	Optimal Specificity	Classification Accuracy
0.5×0.5	0.641	40%	35%	37.50%
1×1	0.753	53%	45%	49.30%
2×2	0.811	63%	65%	64.50%
3×3	0.818	68%	75%	72.70%
4×4	0.869	81%	75%	**78.10**%

We also found the best results at a lower resolution for this dataset as well. In this case, downsampled images (scale factor = 0.125) have the best results. We observed the best classification accuracy (93.50%), the maximum AUC (0.895) and the best optimal sensitivity (94%) and specificity (92%) when the neigh-

Table 10: ROC analysis of Dataset 3 using CoHOG features extracted for neighborhood radius of 8.

Image Pixel Size (mm^2)	Maximum AUC	Optimal Sensitivity	Optimal Specificity	Classification Accuracy
0.5×0.5	0.659	31%	37%	34.20%
1×1	0.780	43%	39%	41.50%
2×2	0.821	75%	74%	74.20%
3×3	0.845	81%	83%	82.00%
4×4	0.895	94%	92%	**93.50**%

borhood size is 8.

For all of the three dataset results, we apply the Sobel operators for gradient orientation calculation. Dataset 1 and 2 are both T2-weighted but are collected from different scanner parameters. Dataset 3 is a T1-weighted dataset which is different from the other datasets. We select the AUC $\geq$ 0.8 for all of the above results because we observe that the best classification results are obtained using AUC$\geq$ 0.8. Fig. 6 shows the classification accuracy for the selected features using different AUC thresholds.

Dataset 1 and two neighborhood sizes are used in this experiment. For both neighborhoods, we found the best classification results at AUC $\geq$ 0.8. Mean feature values and standard deviations of mean feature values of ten selected features of patients and controls using AUC$\geq$0.8 for dataset 1 and dataset 2 are shown in Fig. 7. There is a significant difference between the patients and the controls in the mean feature values and also their standard deviations do not overlap.

We observe that images with lower resolution give better results in classification. This is because the reduced resolution image contains more dense information than the original image for a fixed neighborhood size. With a fixed neighborhood size, CoHOG can cover more regions in feature extraction for downsampled image than for the original image. Thus the extracted features have more distance information for downsampled image than for the original

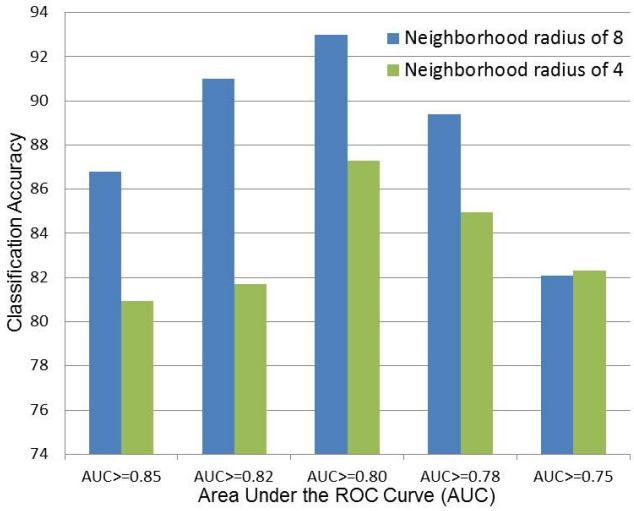

Figure 6: Classification accuracy for selected features using different AUC thresholds for dataset 1.

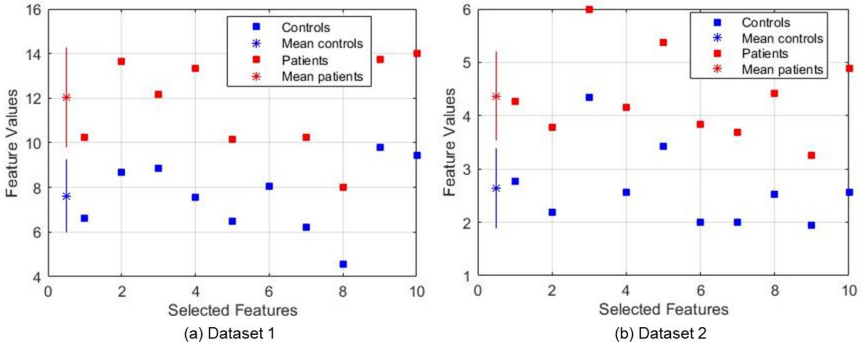

Figure 7: Mean feature values with standard deviations of the mean feature values between patients and controls of ten selected features for (a) Dataset 1 and (b) Dataset 2.

image. For MR dataset 1, the best results are obtained using downsampled images with a pixel size of 3×3 mm^2 and of 4×4 mm^2 give the best results for MR dataset 2 and 3. For all of the MR datasets, the best results are observed using a neighborhood size of 8. Therefore, the rest of the experimental analysis is focused on using only downsampled images with a pixel size of 3×3 mm^2 for MR dataset 1 and of 4×4 mm^2 for MR dataset 2 and 3 with a neighborhood

size of 8.

4.3. ROC Analysis using different Gradient Operators

Three different gradient operators, Sobel, Gaussian Derivative (GD) and Local Frequency Descriptor Gradient (LFDG) are employed to calculate the gradient orientations. Using these operators separately we analyze the classification accuracy and ROC analysis of the dataset 1 and 2. The results of classification accuracy and optimal sensitivity and specificity for dataset 1 are shown in Table 11.

Table 11: ROC analysis of Dataset 1 using three different Gradient Operators. CoHOG features extracted using a neighborhood radius of 8.

Gradient Operators	Maximum AUC	Optimal Sensitivity	Optimal Specificity	Classification Accuracy
Sobel	0.917	91%	95%	93.00%
GD	**0.954**	**98**%	**96**%	**97.30**%
LFDG	0.897	88%	98%	94.75%

All of the three gradient operators have high classification accuracy with optimal sensitivity and specificity. Among them, GD operator has the highest classification accuracy (97.30%) and the optimal sensitivity (98%) and specificity (96%). Also, GD has the highest maximum AUC (0.954) among the all the operators.

Table 12: ROC analysis of Dataset 2 using three different Gradient Operators. CoHOG features extracted using a neighborhood radius of 8.

Gradient Operators	Maximum AUC	Optimal Sensitivity	Optimal Specificity	Classification Accuracy
Sobel	0.867	92%	88%	90.40%
GD	**0.918**	**91**%	**93**%	**92.30**%
LFDG	0.864	87%	95%	91.00%

For dataset 2, the results are shown in Table 12. In this case, GD has a better

performance than the other two methods too. GD operator acquires the highest classification accuracy of 92.30% along with the highest optimal sensitivity of 91% and specificity of 93%.

4.4. Region Based Analysis

In this experiment, we perform region based analysis of the subjects of MR dataset 1. We subdivided the downsampled image with an image pixel size of $3{\times}3\ mm^2$ into 15 equal sized square sub-regions, each of which is of size 10×10 pixels. Now for each sub-region, we apply CoHOG with a neighborhood size of 8 using Sobel operators. Selected features using ROC analysis are applied to the SVM classifier. Based on the classification accuracy, we highlight seven regions that have the highest classification accuracy.

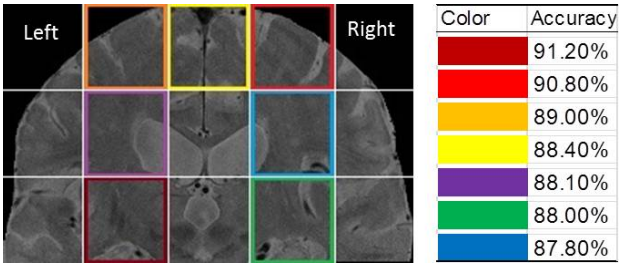

Figure 8: Region based analysis of the subjects of dataset 1. Significant regions are marked by the colored boxes and classification accuracy of the corresponding boxes.

Fig. 8 shows the highlighted regions of the MRI image that have the highest classification accuracy. The classification accuracy of the corresponding colored box is shown in Fig. 8 as well. From the figure, we can see that regions with significant differences between patients and controls correspond to regions most severely affected by ALS, namely the motor cortex and the corticospinal tracts. The top left and right regions contain less tissue in them. These small regions do not have enough texture information to extract features and thus have the lower classification accuracies.

4.5. Comparison with GLCM

We compare the best results of our proposed method with that of the well-known GLCM method. GLCM has been used in medical image analysis in many applications Sivapriya et al. (2011), Li et al. (2010), Kharrat et al. (2009). We implemented the GLCM method (Gray Labels = 32, Neighbor distance = 1, Neighbor direction = 0^0) in the same environment for datasets 1 and 2. In total, 22 features are calculated using well-known feature functions in GLCM. Among them only 3 features namely, Angular second moment, Entropy and Sum entropy are selected using ROC feature selection with an AUC threshold. The results are shown in Table 13 and Table 14 for MR datasets 1 and 2, respectively.

Table 13: Comparison of ROC analysis between CoHOG and GLCM methods using Dataset 1.

Methods	Maximum AUC	Optimal Sensitivity	Optimal Specificity	Classification Accuracy
CoHOG	**0.954**	**98**%	**96**%	**97.30**%
GLCM	0.601	4%	95%	58.60%

Table 14: Comparison of ROC analysis between CoHOG and GLCM methods using Dataset 2.

Methods	Maximum AUC	Optimal Sensitivity	Optimal Specificity	Classification Accuracy
CoHOG	**0.918**	**91**%	**93**%	**92.30**%
GLCM	0.805	68%	76%	72.30%

We found the best results in downsampled images with a pixel size of 3×3 mm^2 and of 4×4 mm^2 for dataset 1 and 2, respectively. The proposed CoHOG method outperforms the GLCM method for both the datasets. For dataset 1, we observe that GLCM has very poor performance. In particular, it has a high specificity but a very low sensitivity. The overall classification accuracy is very low compared to that of CoHOG. Using dataset 2, GLCM has a better performance than using dataset 1, but is still worse than that of CoHOG. Dataset 1

was acquired using a high resolution 4.7 Tesla MRI system and dataset 2 was acquired using a relatively low resolution 1.5 Tesla MRI system. So, we can see from the comparison results that GLCM has a poor performance using high resolution images than that of low resolution images. This is because of its sensitivity to changes in the intensity levels that GLCM uses for features. Such a finding is consistent with the observation that the proposed CoHOG method have very similar performance using either datasets.

5. Conclusion

To the best of our knowledge, we are the first to use the CoHOG method to study cerebral degeneration in ALS. Instead of sub-dividing the image into sub-regions we applied CoHOG with two different neighborhood sizes to the whole image and employed three different gradient operators to calculate the gradient orientation of image pixels. Feature selection was done using ROC analysis and selected features were used for classification. The experimental results demonstrate that our proposed CoHOG method with the accompanying feature selection method has promising classification abilities with high sensitivity and specificity. It outperforms the well-known GLCM texture analysis method. Region based analysis was also performed and revealed that areas most responsible for significant differences between the patients and controls are congruent with the spatial distribution of the pathology of ALS. In summary, the proposed CoHOG method showed excellent classification accuracy in datasets of different contrasts (T1 and T2) and from data collected from two different MRI machines. Thus, texture analysis using CoHOG shows promise as a potential biomarker for ALS and warrants further evaluation in multi-center studies.

Acknowledgment

The authors would like to thank the ALS Society of Canada, ALS Association of America, the MSI Foundation of Alberta, the University of Alberta Hos-

pital Foundation, the Shelly Mrkonjic Foundation, Brain Canada, and NSERC for their generous financial support.

References

References

Albuquerque, M., Anjos, L.G., Maia Tavares de Andrade, H., Oliveira, M.S., Castellano, G., Junqueira Ribeiro de Rezende, T., Nucci, A., Cavalcante França, M., 2016. Mri texture analysis reveals deep gray nuclei damage in amyotrophic lateral sclerosis. Journal of Neuroimaging 26, 201–206.

Alshawabkeh, M., Aslam, J.A., Dy, J., Kaeli, D., 2011. Feature selection metric using auc margin for small samples and imbalanced data classification problems, in: Machine Learning and Applications and Workshops (ICMLA), 2011 10th International Conference on, IEEE. pp. 145–150.

Brooks, B.R., Miller, R.G., Swash, M., Munsat, T.L., 2000. El escorial revisited: revised criteria for the diagnosis of amyotrophic lateral sclerosis. Amyotrophic lateral sclerosis and other motor neuron disorders 1, 293–299.

Chu, X., Chan, K.L., 2009. Rotation and scale invariant texture analysis with tunable gabor filter banks, in: Advances in Image and Video Technology. Springer, pp. 83–93.

Cohen, F.S., Fan, Z., Patel, M.A., 1991. Classification of rotated and scaled textured images using gaussian markov random field models. IEEE Transactions on Pattern Analysis & Machine Intelligence , 192–202.

Cortes, C., Vapnik, V., 1995. Support-vector networks. Machine learning 20, 273–297.

Cross, G.R., Jain, A.K., 1983. Markov random field texture models. Pattern Analysis and Machine Intelligence, IEEE Transactions on , 25–39.

Dalal, N., Triggs, B., 2005. Histograms of oriented gradients for human detection, in: Computer Vision and Pattern Recognition, 2005. CVPR 2005. IEEE Computer Society Conference on, IEEE. pp. 886–893.

Depeursinge, A., Foncubierta-Rodriguez, A., Van De Ville, D., Müller, H., 2014. Three-dimensional solid texture analysis in biomedical imaging: Review and opportunities. Medical image analysis 18, 176–196.

Do, T.T., Kijak, E., 2012. Face recognition using co-occurrence histograms of oriented gradients, in: Acoustics, Speech and Signal Processing (ICASSP), 2012 IEEE International Conference on, IEEE. pp. 1301–1304.

Duda, R.O., Hart, P.E., et al., 1973. Pattern classification and scene analysis. volume 3. Wiley New York.

Galloway, M.M., 1975. Texture analysis using gray level run lengths. Computer graphics and image processing 4, 172–179.

Hanbay, K., Alpaslan, N., Talu, M.F., Hanbay, D., Karci, A., Kocamaz, A.F., 2015. Continuous rotation invariant features for gradient-based texture classification. Computer Vision and Image Understanding 132, 87–101.

Haralick, R.M., Shanmugam, K., Dinstein, I.H., 1973. Textural features for image classification. Systems, Man and Cybernetics, IEEE Transactions on , 610–621.

Hegenbart, S., Uhl, A., Vécsei, A., Wimmer, G., 2013. Scale invariant texture descriptors for classifying celiac disease. Medical image analysis 17, 458–474.

Jafari-Khouzani, K., Siadat, M.R., Soltanian-Zadeh, H., Elisevich, K., 2003. Texture analysis of hippocampus for epilepsy, in: Medical Imaging 2003, International Society for Optics and Photonics. pp. 279–288.

Kassner, A., Thornhill, R., 2010. Texture analysis: a review of neurologic mr imaging applications. American Journal of Neuroradiology 31, 809–816.

Kataoka, H., Hashimoto, K., Iwata, K., Satoh, Y., Navab, N., Ilic, S., Aoki, Y., 2014. Extended co-occurrence hog with dense trajectories for fine-grained activity recognition, in: Computer Vision–ACCV 2014. Springer, pp. 336–349.

Kharrat, A., Benamrane, N., Ben Messaoud, M., Abid, M., 2009. Detection of brain tumor in medical images, in: Signals, Circuits and Systems (SCS), 2009 3rd International Conference on, IEEE. pp. 1–6.

Kiernan, M.C., Vucic, S., Cheah, B.C., Turner, M.R., Eisen, A., Hardiman, O., Burrell, J.R., Zoing, M.C., 2011. Amyotrophic lateral sclerosis. The Lancet 377, 942–955.

Lazebnik, S., Schmid, C., Ponce, J., 2005. A sparse texture representation using local affine regions. Pattern Analysis and Machine Intelligence, IEEE Transactions on 27, 1265–1278.

Lehana, P., Devi, S., Singh, S., Abrol, P., Khan, S., Arya, S., 2012. Investigations of the mri images using aura transformation. Signal & Image Processing 3, 95.

Leung, T., Malik, J., 2001. Representing and recognizing the visual appearance of materials using three-dimensional textons. International journal of computer vision 43, 29–44.

Li, W., Coats, M., Zhang, J., McKenna, S.J., 2015. Discriminating dysplasia: Optical tomographic texture analysis of colorectal polyps. Medical image analysis 26, 57–69.

Li, W.C., Tsai, D.M., 2012. Wavelet-based defect detection in solar wafer images with inhomogeneous texture. Pattern Recognition 45, 742–756.

Li, X., Xia, H., Zhou, Z., Tong, L., 2010. 3d texture analysis of hippocampus based on mr images in patients with alzheimer disease and mild cognitive impairment, in: Biomedical Engineering and Informatics (BMEI), 2010 3rd International Conference on, IEEE. pp. 1–4.

Lorente, D., Blasco, J., Serrano, A., Soria-Olivas, E., Aleixos, N., Gómez-Sanchis, J., 2013. Comparison of roc feature selection method for the detection of decay in citrus fruit using hyperspectral images. Food and Bioprocess Technology 6, 3613–3619.

Lowe, D.G., 2004. Distinctive image features from scale-invariant keypoints. International journal of computer vision 60, 91–110.

Ma, S., Huang, J., 2005. Regularized roc method for disease classification and biomarker selection with microarray data. Bioinformatics 21, 4356–4362.

Maani, R., Kalra, S., Yang, Y.H., 2013. Rotation invariant local frequency descriptors for texture classification. Image Processing, IEEE Transactions on 22, 2409–2419.

Maani, R., Kalra, S., Yang, Y.H., 2014. Robust volumetric texture classification of magnetic resonance images of the brain using local frequency descriptor. Image Processing, IEEE Transactions on 23, 4625–4636.

Maani, R., Yang, Y.H., Emery, D., Kalra, S., 2016. Cerebral degeneration in amyotrophic lateral sclerosis revealed by 3-dimensional texture analysis. Frontiers in Neuroscience 10.

Nanni, L., Lumini, A., 2008. Local binary patterns for a hybrid fingerprint matcher. Pattern recognition 41, 3461–3466.

Ojala, T., Pietikäinen, M., Mäenpää, T., 2002. Multiresolution gray-scale and rotation invariant texture classification with local binary patterns. Pattern Analysis and Machine Intelligence, IEEE Transactions on 24, 971–987.

Qin, X., Yang, Y.H., 2004. Similarity measure and learning with gray level aura matrices (glam) for texture image retrieval, in: Computer Vision and Pattern Recognition, 2004. CVPR 2004. Proceedings of the 2004 IEEE Computer Society Conference on, IEEE. pp. I–326.

Reyes-Aldasoro, C.C., Bhalerao, A., 2006. The bhattacharyya space for feature selection and its application to texture segmentation. Pattern Recognition 39, 812–826.

Santos, J.A.d., Gosselin, P.H., Philipp-Foliguet, S., Torres, R.d.S., Falao, A.X., 2012. Multiscale classification of remote sensing images. Geoscience and Remote Sensing, IEEE Transactions on 50, 3764–3775.

Serrano, A.J., Soria-Olivas, E., Martín-Guerrero, J.D., Magdalena, R., Gomez, J., 2010. Feature selection using roc curves on classification problems., in: IJCNN, pp. 1–6.

Sivapriya, T., Saravanan, V., Thangaiah, P.R.J., 2011. Texture analysis of brain mri and classification with bpn for the diagnosis of dementia, in: Trends in Computer Science, Engineering and Information Technology. Springer, pp. 553–563.

Unser, M., Eden, M., 1989. Multiresolution feature extraction and selection for texture segmentation. Pattern Analysis and Machine Intelligence, IEEE Transactions on 11, 717–728.

Varma, M., Zisserman, A., 2005. A statistical approach to texture classification from single images. International Journal of Computer Vision 62, 61–81.

Watanabe, T., Ito, S., Yokoi, K., 2009. Co-occurrence histograms of oriented gradients for pedestrian detection, in: Advances in Image and Video Technology. Springer, pp. 37–47.

Zhang, J., Zhao, H., Liang, J., 2013. Continuous rotation invariant local descriptors for texton dictionary-based texture classification. Computer Vision and Image Understanding 117, 56–75.

Zhao, M., Li, S., Kwok, J., 2010. Text detection in images using sparse representation with discriminative dictionaries. Image and Vision Computing 28, 1590–1599.

Biography

G M Mashrur E Elahi received the B.Sc. Engineering degree (with honors) in computer science & engineering from Khulna University of Engineering & Technology, Khulna 9203, Bangladesh, in 2009. He is currently pursuing the M.Sc degree with the Department of Computing Science, University of Alberta, Edmonton, AB, Canada. He has published two International Journals and three International Conference papers. His current research interests include computer vision, image processing, and medical image analysis. He is an Associate Member of the Institute of Engineers Bangladesh (IEB).

Sanjay Kalra obtained his MD at the University of Toronto, neurology specialty training at McGill University, and completed a research fellowship at the Montreal Neurological Institute. He is currently a professor in the Division of Neurology, Department of Medicine, holds adjunct appointments in the departments of Computing Science and Biomedical Engineering, and is a member of the Neuroscience and Mental Health Institute. His research focuses on the development and application of advanced magnetic resonance imaging techniques to study amyotrophic lateral sclerosis.

Yee-Hong Yang (SM IEEE) received his B.Sc. (first honors) from the University of Hong Kong, his M.Sc. from Simon Fraser University, and his M.S.E.E. and Ph.D. from the University of Pittsburgh. He was a faculty member in the Department of Computer Science at the University of Saskatchewan from 1983 to 2001 and served as Graduate Chair from 1999 to 2001. Since July, 2001, he has been a Professor in the Department of Computing Science at the University of Alberta. He served as Associate Chair (Graduate Studies) in the same department from 2003 to 2005.

His research interests cover a wide range of topics from computer graphics to computer vision, which include physically based animation of Newtonian and non-Newtonian fluids, texture analysis and synthesis, human body motion analysis and synthesis, computational photography, stereo and multiple view computer vision, and underwater imaging. He has published over 100 papers

in international journals and conference proceedings in the areas of computer vision and graphics. He is a Senior Member of the IEEE and serves on the Editorial Board of the journal Pattern Recognition. In addition, he has served as reviewer to many international journals, conferences, and funding agencies, and on program committees of many national and international conferences. In 2007, he was invited to serve on the expert review panel to evaluate computer science research in Finland. He is currently serving as the Science Internship Program Director in the Department of Computing Science.